

Energy partition in two solar flare/CME events

A. G. Emslie,¹ H. Kucharek,² B. R. Dennis,³ N. Gopalswamy,⁴ G. D. Holman,³
G. H. Share,⁵ A. Vourlidas,⁶ T. G. Forbes,² P. T. Gallagher,^{3,7} G. M. Mason,⁸
T. R. Metcalf,⁹ R. A. Mewaldt,¹⁰ R. J. Murphy,⁵ R. A. Schwartz,^{3,11} and T. H. Zurbuchen¹²

Received 30 April 2004; revised 12 July 2004; accepted 6 August 2004; published XX Month 2004.

[1] Using coordinated observations from instruments on the Advanced Composition Explorer (ACE), the Solar and Heliospheric Observatory (SOHO), and the Ramaty High Energy Solar Spectroscopic Imager (RHESSI), we have evaluated the energetics of two well-observed flare/CME events on 21 April 2002 and 23 July 2002. For each event, we have estimated the energy contents (and the likely uncertainties) of (1) the coronal mass ejection, (2) the thermal plasma at the Sun, (3) the hard X-ray producing accelerated electrons, (4) the gamma-ray producing ions, and (5) the solar energetic particles. The results are assimilated and discussed relative to the probable amount of nonpotential magnetic energy available in a large active region. **INDEX TERMS:** 7519 Solar Physics, Astrophysics, and Astronomy: Flares; 7513 Solar Physics, Astrophysics, and Astronomy: Coronal mass ejections; 7514 Solar Physics, Astrophysics, and Astronomy: Energetic particles (2114); 7554 Solar Physics, Astrophysics, and Astronomy: X rays, gamma rays, and neutrinos; **KEYWORDS:** solar flares, coronal mass ejections, solar energetic particles, energetics, hard X rays, gamma rays

Citation: Emslie, A. G., et al. (2004), Energy partition in two solar flare/CME events, *J. Geophys. Res.*, 109, XXXXXX, doi:10.1029/2004JA010571.

1. Introduction

[2] Solar flares and coronal mass ejections (CMEs) are the most powerful events in the solar system. In tens of minutes they can convert in excess of 10^{32} ergs of magnetic energy into accelerated particles, heated plasma, and ejected solar material. While the order of magnitude of this total energy is not in serious doubt, its partition amongst the component parts of the flare and CME has yet to be reliably evaluated for a particular event or set of events. A reliable estimate of this partition, and of its variation from event to

event would provide powerful constraints on the energy release process(es) at work.

[3] Various previous studies have examined the energy budget of a limited number of energy components in certain flares. For example, *Canfield et al.* [1980] evaluated the radiative energy budget of a solar flare on 5 February 1973. However, without the benefit of hard X-ray or gamma-ray observations, they were not able to make an assessment of the role of energetic particles in the event. Neither were they able to assess the kinetic energy in the confined flare plasma, in any associated coronal mass ejection, or in accelerated interplanetary particles. *Strong et al.* [1984] assessed the energy contents in thermal plasma, nonthermal electrons, and hydrodynamic mass motions of nonejected material for two flares within the same active region on 31 August 1980. Most recently, *Saint-Hilaire and Benz* [2002] presented an energy budget for a compact flare that occurred on 20 February 2002. They included the thermal and radiative energy of the flare plasma, the nonthermal electron beam energy, and the kinetic energy of the non-CME-associated plasma ejecta. Neither of these latter studies, however, were able to include an assessment of the energy content in accelerated ions, nor did they attempt an evaluation of the energies in the CME, interplanetary shock, or accelerated interplanetary particles.

[4] Our observational database with which to address questions of flare/CME energetics has steadily improved over time, to the point where a more comprehensive assessment of the energy content of various components of the flare is now possible. For example, observations of CMEs are available on a continuous duty cycle from the LASCO instrument on the SOHO spacecraft. Estimates of 64

¹Department of Physics, University of Alabama in Huntsville, Huntsville, Alabama, USA.

²Institute for the Study of Earth, Oceans, and Space, University of New Hampshire, Durham, New Hampshire, USA.

³Code 682, NASA Goddard Space Flight Center, Greenbelt, Maryland, USA.

⁴Code 695, NASA Goddard Space Flight Center, Greenbelt, Maryland, USA.

⁵Code 7650, Naval Research Laboratory, Washington, DC, USA.

⁶Code 7663, Naval Research Laboratory, Washington, DC, USA.

⁷Also at L-3 Communications GSI, New York, USA.

⁸Department of Physics, University of Maryland, College Park, Maryland, USA.

⁹Lockheed Martin Solar and Astrophysics Laboratory, Palo Alto, California, USA.

¹⁰California Institute of Technology, Pasadena, California, USA.

¹¹Also at Science Systems and Applications, Inc., Lanham, Maryland, USA.

¹²Department of Atmospheric, Oceanic, and Space Sciences, University of Michigan, Ann Arbor, Michigan, USA.

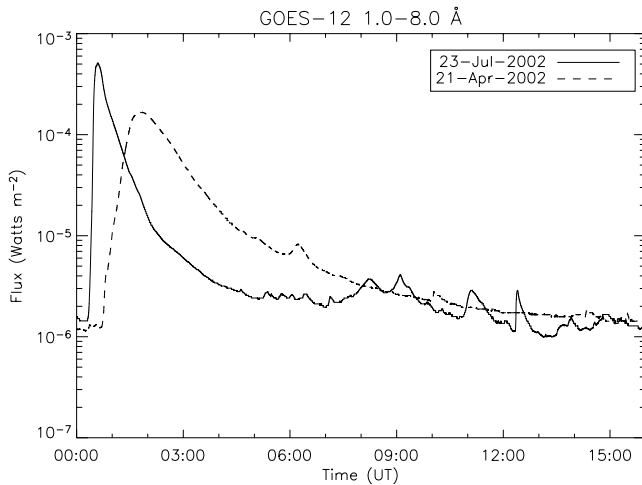


Figure 1. GOES 1–8 Å light curves for the two events studied. The zero of the time axis coincides with 0000 UT on each date.

the energy in accelerated charged particles and in the flare thermal plasma can be made through interpretation of the X-ray and gamma ray signatures observed by the Ramaty High Energy Solar Spectroscopic Imager (RHESSI). Finally, the Advanced Composition Explorer (ACE) suite of instruments provides information on the energy in accelerated interplanetary particles.

[5] From 7 to 9 October 2003 a workshop was held in Taos, New Mexico to investigate problems of common interest to investigators working on data from the ACE, RHESSI, and Wind missions. Working Group 5 at that workshop addressed the task of evaluating the energetics of the various components in two well-observed flare/CME events, a GOES X1.5 flare on 21 April 2002 and an X4.8 event on 23 July 2002; this paper is the result of that collaboration.

[6] Figure 1 shows the GOES soft X-ray light curves for the two events studied. The 21 April event was a long-lived soft X-ray event, with significant 1–8 Å flux observable over 12 hours after the flare onset; it occurred near the west limb at S14W84. Its overall properties have been discussed by *Gallagher et al.* [2002]. By contrast, the 23 July event was much more impulsive, was a strong emitter of hard X rays and gamma rays [see *Lin et al.*, 2003], and was located near the east limb at S13E72.

[7] In section 2 we consider the energetics of the CMEs associated with these events. In section 3 we evaluate the energetics of the hot, soft X-ray emitting plasma produced during the flare and that of hard X-ray producing accelerated electrons. In section 4 we turn our attention to the energetics of accelerated ions. In section 5 we consider the energetics of the interplanetary particles commonly believed to have been accelerated by the CME-associated shock. In section 6 we consider the available energy in stressed magnetic fields. In section 7 we summarize the results in tabular form and discuss their significance.

2. CME Energetics

[8] Coronal mass ejections for both the 21 April 2002 and 23 July 2002 events were well observed by both the

LASCO C2 and C3 coronagraphs [*Brueckner et al.*, 1995] on SOHO [*Domingo et al.*, 1995] (Figure 2). A detailed analysis of the propagation of the 21 April CME through the corona as observed by TRACE, UVCS, and LASCO is given by *Gallagher et al.* [2003].

[9] With the use of calibrated LASCO images, we can derive estimates of the kinetic and potential energy of the two CMEs. The procedure is as follows: First, we select an image containing the CME and a preevent image, as close in time as possible to the flare, which does not show any disturbances or ejecta over the path of the subsequent CME. Next, the images are calibrated (in units of mean solar brightness) and the preevent image is subtracted from the CME image. The excess brightness revealed by this subtracted image is due to Thompson scattering of photospheric radiation from the excess mass in the CME.

[10] The excess brightness is then converted to the excess mass of the CME under the usual assumptions [*Poland et al.*, 1981; *Vourlidas et al.*, 2000, 2002] as follows: (1) all of the CME mass is concentrated on the plane of the sky, and (2) the CME material consists of 90% H and 10% He. We invoke the first assumption because the true three-dimensional distribution of the CME mass along the line of sight is unknown. It is a very good assumption here, since both of our CMEs originated from regions very close to the limb and are very likely propagating along the sky plane. The second assumption represents an “average” coronal composition since we do not know the height at which the bulk of the CME material originates (other than that it is coronal).

[11] These assumptions together result in an uncertainty about the true mass of a CME which becomes more significant as the central angle and/or spread of a given CME departs significantly from the sky plane. The mass uncertainty is about a factor of 2 for CMEs that are 40 degrees from the sky plane [*Vourlidas et al.*, 2000]. Generally speaking, one should be aware of other uncertainties in this procedure that include exposure time variations between event and preevent images, improper vignetting correction, solar rotation effects, and the presence of stars in the field of view. Fortunately, such uncertainties can be minimized to a level that is well below that of other factors through proper calibration and careful choice of event and preevent images, as we have done here.

[12] After obtaining a series of excess mass images of the CME as a function of time, we can compute the total mass of the CME and the position and projected velocity of both the leading edge and the center of mass of the CME. From the mass, projected velocity, and position data follow estimates of the total kinetic (U_K) and potential (U_Φ) energies [*Vourlidas et al.*, 2000]. Thus one can, in principle, follow the evolution of the energy and mass as the CME propagates outward in the corona. However, while this is possible for the majority of LASCO CMEs, it is not the case for the two events considered here, which both move very quickly through the C2 field of view, leaving only the C3 images for analysis. Moreover, in the 21 April event, high intensities of energetic particles reached the SoHO spacecraft within less than an hour of the flare peak; these particles produced large numbers of solar particle hits on the LASCO detectors, making later images unusable for

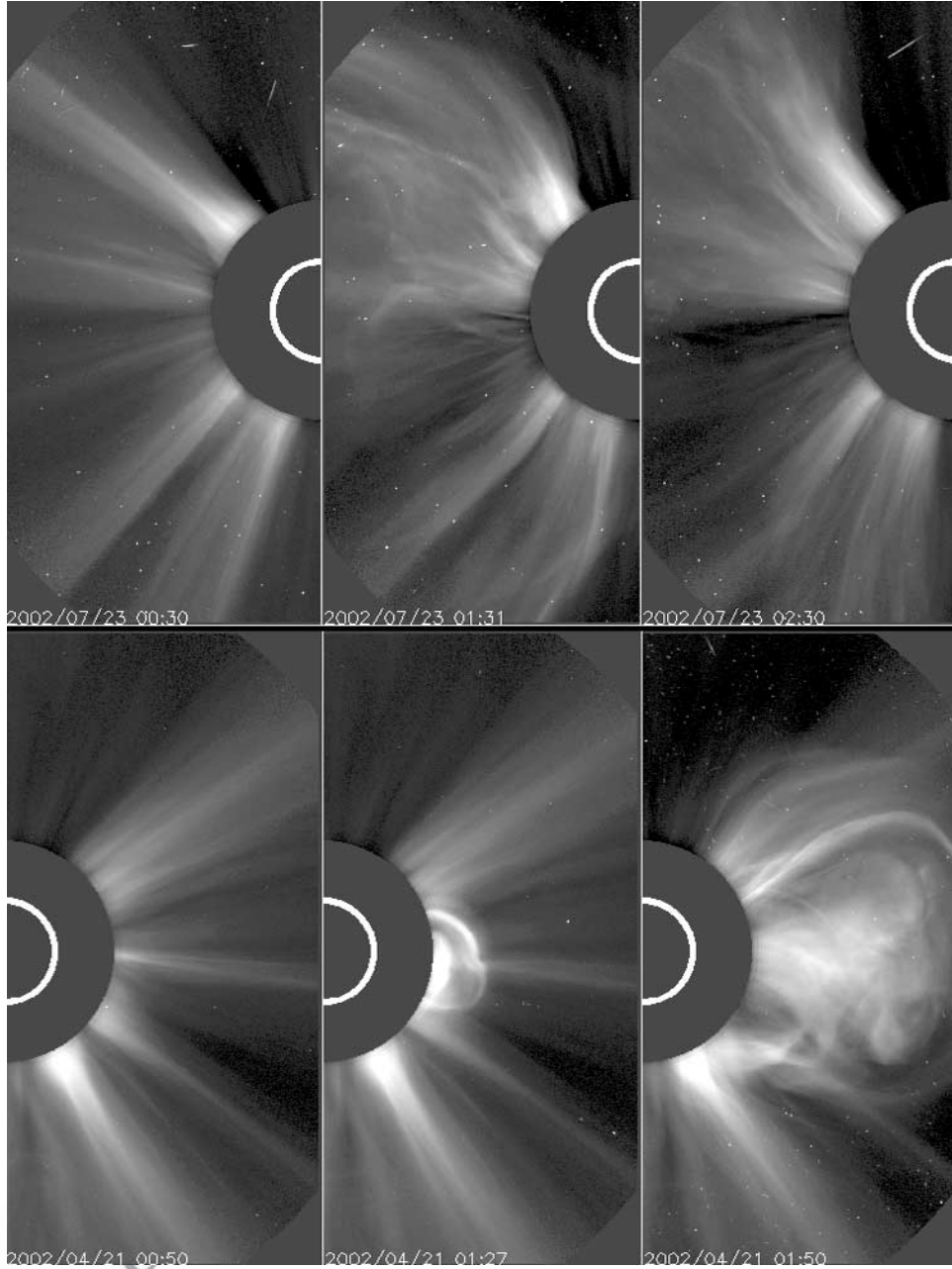


Figure 2. LASCO/C2 observations of the 23 July (top) and 21 April 2002 (bottom) flare/CME events. The configuration of the preevent corona is shown in the leftmost panels. The CMEs were very fast so only a couple of C2 images are available. The observation times are shown on the figures.

quantitative analysis. For these reasons, we are only able to provide mass and energy measurements from the LASCO/C3 image that shows all (or at least most) of the event mass during the period when solar particle hits were not a significant factor.

[13] Table 1 shows the mass and the projected velocities at $10R_{\odot}$ and $18R_{\odot}$, respectively, at 0218 UT for each event, as well as estimates for the associated kinetic and potential energies. Note that the 21 April event was an accelerating event, and a second-order fit to the position data yields a

Table 1. LASCO CME Measurements

Event	Mass, 10^{15} g	Speed at $10R_{\odot}$, km s^{-1}	Speed at $18R_{\odot}$, km s^{-1}	Kinetic Energy U_K , 10^{30} erg	Potential Energy U_{Φ} , 10^{30} erg
21 April 2002	2.8	2300	2700	180	4.6
23 July 2002	7.1	2600	2000	110	12

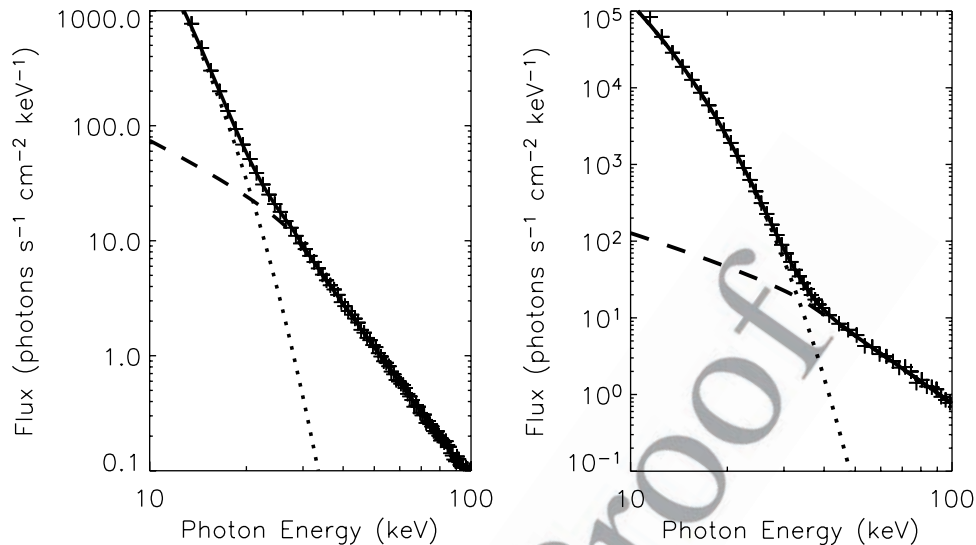


Figure 3. Sample RHESSI spectra and fits for the 21 April 2002 (left) and 23 July 2002 (right) flares. The plus signs denote the data points. The data were fit from 15 keV to 100 keV with the bremsstrahlung from an isothermal plasma (dotted curve) and the bremsstrahlung from a double-power-law mean electron flux distribution with a low-energy cutoff (dashed curve). The solid curve, the best-fit spectrum, is the sum of these two spectra. The time intervals are 0115:00–0116:00 UT for the 21 April spectrum and 0035:00–0036:00 UT for the 23 July spectrum.

mean acceleration of 156 m s^{-2} , two orders of magnitude larger than the solar gravitational acceleration at this distance. By contrast, the 23 July event first accelerates and then quickly decelerates in the LASCO/C3 field of view. Consequently, no single value provides an adequate characterization of the acceleration profile for this event.

[14] These results further reinforce our notion that these are unusual CME events. Their large kinetic energies place both of them in the top 1% of all observed CMEs for the period 1996–2000 [Vourlidis *et al.*, 2002]. In both cases, the gravitational potential energy is only some 10% of the total energy contained in the CME. The uncertainties in these values are dominated by the uncertainty in the mass and are estimated to be a factor of ~ 2 .

3. Energetics of the Thermal Plasma and Accelerated Electrons

[15] The energy content of both the hottest thermal plasma and the accelerated (nonthermal) electrons can be derived from the RHESSI X-ray images and spectra. We choose to treat these two components separately even though this results in some double budgeting, since the nonthermal electrons will contribute to the plasma heating as they lose their energy by Coulomb collisions. This is expected to be most significant when the Neupert Effect (after Neupert [1968]) is obvious from the light curves [Dennis *et al.*, 2003].

[16] In the impulsive phase of both flares studied here, a thermal component is clearly visible in the X-ray spectra at the lowest photon energies (Figure 3). A flatter extension to higher energies is interpreted as bremsstrahlung emission from a nonthermal electron beam in a thick target. We used a parametric isothermal plus a double power law function for the mean source electron spectrum $\bar{F}(E)$ [Brown *et al.*,

2003] in conjunction with the bremsstrahlung cross section of Haug [1997] to fit the observed hard X-ray spectrum [Holman *et al.*, 2003]. The results presented here were obtained from a sequence of $\bar{F}(E)$ spectra calculated for contiguous 20-s intervals throughout each flare using X-ray flux measurements above 10 keV, where the RHESSI spectral response is best known.

3.1. Hot Plasma

[17] We have carried out an analysis of the thermal plasma similar to that reported by Moore *et al.* [1980] and Strong *et al.* [1986]. The energy going into plasma heating during each flare was estimated by computing the time evolution of the energy content of the thermal plasma and obtaining the peak value. This constitutes a lower limit to the thermal energy, since it does not account for the cooling of the plasma prior to this time nor to any heating at later times. Each of these additional contributions are considered separately below; they are believed to add perhaps a factor of 3 to the peak thermal energy. No attempt was made to determine the kinetic energy of turbulent and directed plasma motions, since no spectrally resolved lines were available to give a measure of line broadening caused by such bulk motions. For other flares observed with the Bragg Crystal Spectrometers on SMM and Yohkoh, the energy in this component has generally been estimated to be a small fraction of the thermal energy in the plasma [Strong *et al.*, 1986].

[18] The thermal energy of the heated plasma was obtained from the temperature T_0 (K) and emission measure $EM = \int n_e^2 dV$ (cm^{-3}) for the thermal portion of the spectral fit. Here n_e is the electron density (cm^{-3}) and V is the emitting volume (cm^3). Account must be taken of the filling factor f equal to the ratio of the emitting volume to the apparent volume (V_{ap}) as determined with an imaging

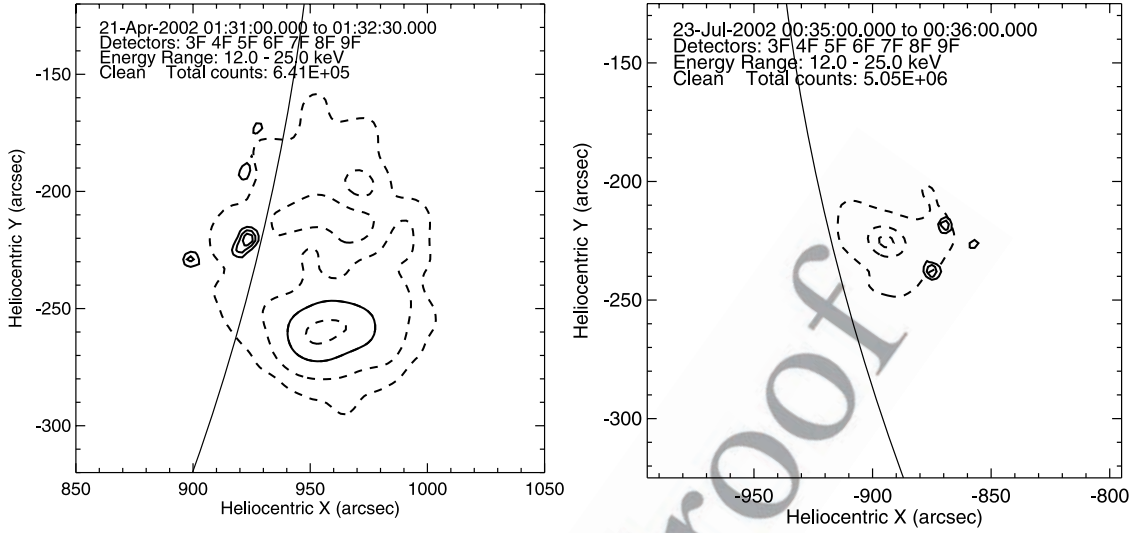


Figure 4. RHESSI images for (left) the flare on 21 April 2002 at 0131:00–0132:30 UT and (right) the flare on 23 July 2002 at 0035:00–0036:00 UT. Both images were obtained using the CLEAN reconstruction algorithm. They correspond to the time of peak soft X-ray emission when all the shutters were in the RHESSI detector fields of view for both events. The 12–25 keV contours are labeled as follows: (left) 10% (broken), 20% (broken), 50% (solid), and 90% (broken); (right) 20%, 50%, and 90% (all broken). The 30–100 keV contours are solid in both images and correspond to 40, 60, and 80% of peak value. The curved line shows the solar limb in each image.

instrument having limited spatial resolution. The thermal energy content of the plasma is then given by the following expression [e.g., *de Jager et al.*, 1986]:

$$U_{\text{th}} = 3 n_e k T_0 f V_{\text{ap}} \simeq 4.14 \times 10^{-16} T_0 \sqrt{EM \times f V_{\text{ap}}} \text{ erg}, \quad (1)$$

where k is Boltzmann’s constant.

[19] We estimated the source volume from the area information obtained from the RHESSI observations. However, it is nontrivial to determine the area of a source from the RHESSI measurements of the modulated flux with its nine collimators with different spatial scales. We have used the technique for doing this for a single symmetrical source described by *Schmahl and Hurford* [2002]. In this technique the modulation amplitude is determined for each of the collimators and the rotationally averaged size determined that would give that distribution of values. For the 21 April flare at 0131 UT, the FWHM of the 12–25 keV source determined in this way was 26 arcsec, giving a source area of $\pi \times (13)^2 = 530 \text{ arcsec}^2$. This is consistent with the area of the 50% contour of the 12–25 keV image shown in Figure 4 that was produced from the RHESSI data using the CLEAN reconstruction algorithm [*Hurford et al.*, 2002].

[20] This image and the distribution of modulation amplitudes both show that a more extended source was also present with a factor of ~ 10 smaller brightness extending out to sizes possibly as large as 180 arcsec, the largest source that will still produce modulation through RHESSI’s coarsest collimators. Its location and extent match the emission seen in the TRACE images at the same time. From the 12–25 keV image shown in Figure 4, we estimate that the area of the extended source was $3 \times 10^4 \text{ arcsec}^2$ and that it produced approximately 1/3 of the total emission.

Hence it must have contained twice as much thermal energy as the compact source.

[21] For the 23 July 2002 flare between 0035 and 0036 UT, the *Schmahl and Hurford* [2002] method gives a source FWHM of 16 arcsec, a value matched by the area within the 50% contour of the 12–25 keV image shown in Figure 4. In this case, no significant extended source is evident in the distribution of modulation amplitudes or in the reconstructed image.

[22] We estimated the source volumes from the areas A (cm^2) discussed above assuming $V_{\text{ap}} = A^{3/2}$ and a filling factor of unity ($f = 1$). *Aschwanden and Parnell* [2002] have suggested, based on their fractal analysis of flare geometry, that the relation $V_{\text{ap}} = A^{1.3 \pm 0.1}$ may be a better way to determine the flare volume from the measured area. However, for the large flares considered here, this empirical formula results in unreasonable density estimates (as high as 10^{13} cm^{-3}) and so we have not used this expression.

[23] Application of equation (1) to the 21 April and 23 July events yields values of $U_{\text{th}} = 1.3 \times 10^{31} \text{ ergs}$ (including the extended source) and $7 \times 10^{30} \text{ ergs}$, respectively. Since both EM and T_0 are well determined observationally, the principal uncertainties in these values arise from uncertainties in the filling factor f and the apparent volume V_{ap} . From equation (1) and the relation $V_{\text{ap}} = A^{3/2}$, we may write

$$\Delta \log U_{\text{th}} = \sqrt{\left(\frac{1}{2} \Delta \log f\right)^2 + \left(\frac{3}{4} \Delta \log A\right)^2}. \quad (2)$$

With an estimate of $\Delta \log A = \pm 0.5$ and $\Delta \log f = [+0, -2]$ (a filling factor between 1% and unity), we obtain $\Delta \log U_{\text{th}} = [+0.4, -1]$.

[24] More sophisticated fits using a differential emission measure distribution with temperature $DEM(T) \equiv n_e^2 dV/dT$ (e.g., $\propto T^{-\alpha}$) will be used in future work as the RHESSI spectral analysis becomes more capable and our knowledge of the instrument response matrix improves in the different attenuator states. Also, extending the spectral fits to energies below 10 keV, down to RHESSI's lower limit near 3 keV, will provide better estimates of the thermal spectrum at lower temperatures. This will allow the exploitation of the iron and nickel line complexes at ~ 6.7 keV and ~ 8 keV that can be measured with RHESSI's ~ 1 keV FWHM energy resolution [Phillips, 2004].

[25] An estimate of the energy in the hot flare plasma can also be obtained from GOES soft X-ray data. The GOES instruments provide X-ray fluxes in two broad bands, 1.6–12 keV and 3–25 keV. The ratio of the fluxes in these bands and the X-ray intensity provide an estimate of the flare temperature and emission measure, respectively. The thermal energy can then be estimated from equation (1). Since the hard X-ray energies observed with the GOES detectors are lower than the lowest energies observed with RHESSI, the GOES detectors tend to be sensitive to somewhat lower temperature plasma than RHESSI. When RHESSI spectral fits indicated a temperature of 37 MK for the 23 July flare, for example, the temperature deduced from the GOES data was 27 MK. The peak thermal energies deduced from the GOES results for the 21 April and 23 July flares were 1×10^{31} erg in both cases, i.e., comparable to the values obtained with RHESSI.

[26] In addition to the peak energy content of the thermal plasma, a comprehensive assessment of the thermal energy must also include estimates of the energy losses by conduction and radiation during the flare and of any additional energy release during the decay phase of the flare. Conductive cooling is difficult to estimate since, during the impulsive phase at least, a collision-dominated conduction expression is probably not valid [see, e.g., Smith and Lilliequist, 1979]. A. M. Veronig et al. (The Neupert effect: A comparison of data and theory using RHESSI and GOES observations, submitted to *Astrophysics Journal*, 2004, hereinafter referred to as Veronig et al., submitted manuscript, 2004) however, suggest that conductive cooling can result in an energy loss for other flares that is greater than the peak thermal energy content of the plasma. However, for the flares considered here, the simple model they assume is not applicable given the obvious complexity of the magnetic field and the involvement of multiple loop structures. Future work using the multiple loop modeling done by Reeves and Warren [2002] may be able to make realistic estimates of the conductive cooling term, at least for the decay phases of these flares.

[27] Radiative losses are much easier to estimate since they depend only on the emission measure, temperature, and composition of the emitting plasma. We have estimated their magnitude using the standard radiative loss function in the Chianti code, assuming coronal abundances. Assuming that radiation was the only cooling mechanism, the additional energy required to maintain the plasma with the measured emission measure and temperature during the

decay phase of the flare was estimated from the GOES data and found to be 1.8×10^{31} ergs for the 21 April 2002 flare and 1.3×10^{31} ergs for the 23 July 2002 flare.

3.2. Accelerated Electrons

[28] The energy in accelerated electrons was determined from the power law extension to the measured X-ray spectrum assuming a thick target model. In this model the accelerated electrons ultimately lose all of their suprathermal energy through collisions with ambient thermal electrons. The injected electron energy spectrum $F_0(E_0)$ (electrons $\text{cm}^{-2} \text{s}^{-1} \text{keV}^{-1}$) required to produce the inferred mean source spectrum $\bar{F}(E)$ in a collisional cold target is [Brown and Emslie, 1988]

$$F_0(E_0) = \frac{K}{A_i} \left(\frac{\bar{F}(E)}{E^2} \left[1 - \frac{d \ln \bar{F}}{d \ln E} \right] \right)_{E=E_0}, \quad (3)$$

where A_i is the electron injection area (cm^2) and $K = 2\pi e^4 \Lambda$, e being the electronic charge and Λ the Coulomb logarithm appropriate to the ionization state of the target (see below). The corresponding injected energy (ergs) is

$$\begin{aligned} U_e &= A_i \int_t \int_{E_{\min}}^{\infty} E_0 F_0(E_0) dE_0 dt \\ &= K \int_t \int_{E_{\min}}^{\infty} \frac{\bar{F}(E_0)}{E_0} \left[1 - \frac{d \ln \bar{F}(E_0)}{d \ln E_0} \right] dE_0 dt. \end{aligned} \quad (4)$$

Note that the value of the injection area A_i cancels between equations (3) and (4); the electron energy is determined from the time integral of the total hard X-ray flux without the need to assume a value for A_i . Also, the accumulated energy, obtained by integrating the calculated injected electron power over time, was in practice calculated by summing over all the discrete 20-s time intervals for which spectra were obtained.

[29] The above equations assume a cold target in the sense that the thermal electrons have a mean energy (kT) that is significantly lower than the lowest energy of the nonthermal beam electrons. In addition, consideration must be given to the ionization state of the target since the bremsstrahlung efficiency (ergs of hard X rays produced per erg of injected electron energy) is a factor of ~ 3 times lower for a fully ionized plasma than for a neutral target, a consequence of the reduced Coulomb logarithm, and so lower collisional loss rate, appropriate [Brown, 1973; Emslie, 1978]. Since most of the beam energy is in the lower-energy electrons that stop higher in the corona, we used a Coulomb logarithm parameter appropriate for a fully ionized plasma to calculate the total nonthermal energy. A more refined calculation is possible using the procedure outlined by Kontar et al. [2002], but no significant difference is expected in the result.

[30] In our analysis we used a form $F_0(E_0) \propto E_0^{-\alpha}$ between a low-energy cutoff, E_{\min} , and a break energy, E_{brk} , and $F_0(E_0) \propto E_0^{-\beta}$ above E_{brk} . For the 21 April flare, only a single power law index, α , was required to fit the X-ray data. In the thick target model, this results in an X-ray spectrum of the form $I(\epsilon) \propto \epsilon^{-\gamma}$ above $\epsilon_{\min} = E_{\min}$, where ϵ is the X-ray photon energy and $\gamma = \alpha - 1$. The X-ray spectrum flattens below ϵ_{\min} [see Holman, 2003]. The full

double power law fit was required for the 23 July flare. The photon spectrum below E_{brk} is steeper than $\alpha - 1$ because of the reduced number of electrons above E_{brk} [Holman, 2003].

[31] The calculated values of α for the 21 April flare range from 4.5 to 8.5, and for the 23 July flare α ranges from 2 to 8 and β ranges from 4 to 9 [e.g., Holman et al., 2003]. Because of the steep form of these electron distributions, the value of U_e is particularly sensitive to the lower cutoff value E_{min} in equation (4). However, since thermal emission dominates the low-energy part of the photon spectrum as discussed above, the value of E_{min} cannot be directly determined. E_{min} can, in principle, be determined using RHESSI's imaging spectroscopy. By obtaining spectra of nonthermal X-ray sources that are spatially separated from the thermal sources, the nonthermal spectrum should be independently determined without thermal contamination. However, the RHESSI images herein have a limited dynamic range of $\sim 10:1$ because of the Fourier imaging technique that is used and uncertainties in the knowledge of the grid modulation characteristics; the dynamic range will improve as these characteristics are better determined. This limitation and the steepness of the spectra prevent the nonthermal sources from being visible at energies much below the energy at which the steep thermal spectrum begins to dominate. Therefore we could not deduce the value of the low-energy cutoffs from the imaged spectra.

[32] Since the thermal spectrum is so dominant at low energies, the nonthermal power-law part of the electron spectrum can be extended down to arbitrarily low energies while still maintaining an acceptable fit to the overall spectrum. We therefore chose the largest value of E_{min} that still gave an acceptable fit (normalized $\chi^2 \simeq 1$) to the spatially integrated spectral data; as a result, the energies we obtain are necessarily lower limits to the energy in the nonthermal electrons. This is in contrast to previous work where a constant energy is chosen for the value of the low-energy cutoff (for example, Saint-Hilaire and Benz [2002] fixed the low-energy cutoff at 10 keV).

[33] Early in the 23 July flare, before the impulsive rise, there was no obvious transition from predominantly thermal (i.e., steep, concave downward in log-log space) to predominantly nonthermal (i.e., shallow, near straight line in log-log space) forms of photon spectra. This is often the case early in a flare. Instead, we found that the data could be fitted with double power law photon spectra alone and therefore were consistent with pure nonthermal emission. However, this led to unreasonably high energy contents very early in the preimpulsive phase [Holman et al., 2003]. The combination of an isothermal spectrum and a double power law with a low-energy cutoff provides an equally good fit to the data. Thus in keeping with the philosophy of minimizing the energy in nonthermal electrons, the data were fitted with this combined isothermal/nonthermal model. (An alternative possibility, that this early emission was multithermal, will also be considered once the RHESSI spectral analysis is developed to allow fluxes below 10 keV to be reliably included in the fits.) Values of E_{min} ranged from a low of 18 keV to a high of 75 keV [see Holman et al., 2003]. Throughout most of the event, E_{min} ranged from 20 to 40 keV.

[34] Veronig et al. (submitted manuscript, 2004) have calculated the value of E_{min} based on the energy required to produce the observed soft X-ray plasma, through a generalization of the analysis of the Neupert Effect. Values of E_{min} determined by this method, applied to four other flares in April 2002, lie in the range 15–30 keV, consistent with our findings.

[35] For the 23 July event, the electron energy determined by this method was found to be $U_e = 3 \times 10^{31}$ erg. The result for the 21 April event was $U_e = 2 \times 10^{31}$ erg. Despite uncertainties (which we estimate are approximately half an order of magnitude, originating mainly in the determination of E_{min}), these results are, somewhat surprisingly, higher than the corresponding values of 1.3×10^{31} erg and 7×10^{30} erg for the energy contained in the thermal plasma U_{th} . This surprising result is reinforced by the wide lower error bar on U_{th} caused by the uncertain filling factor f and the fact that U_e may be an underestimate. It will be interesting to see if this result holds for other flares.

4. Energetics of Accelerated Ions

[36] Accelerated ions are energetically important in large solar flares with significant emission above ~ 300 keV [Ramaty and Mandzhavidze, 2000]. They manifest themselves principally through the production of gamma-ray lines in the range ~ 1 –10 MeV [e.g., Ramaty et al., 1979]. We plot the time-integrated γ -ray count spectrum of the 23 July 2002 flare in Figure 5, along with the best overall fit and the best-fitting bremsstrahlung and total nuclear components. The nuclear component is composed of moderately broadened lines produced by p and α reactions on ambient C, O, Ne, etc., and highly broadened lines from accelerated C, O, Ne, etc., ion reactions on ambient H and He (an unresolved nuclear continuum merges with this broad component). The flux in the highly broadened component is typically $>3\times$ that in the moderately broadened component.

[37] Since nuclear states producing spectral lines have different excitation thresholds, the ratio of line intensities provides information on the ratio of ion fluxes at different energies, i.e., on the shape of the accelerated ion spectrum. There is a small dependence on the angular distribution of accelerated ions that pales in comparison with the uncertainty in spectral shape. For the 23 July flare we used intensities of the moderately Doppler-broadened ^{12}C (4.43 MeV) deexcitation line, the total nuclear deexcitation line complex from 4 to 7 MeV, and the neutron-capture line at 2.223 MeV. Assuming an ion spectrum of the form $F(E) \sim E^{-\beta}$, we found that β ranged between ~ 3.5 and 4.5 [Lin et al., 2003].

[38] Because the threshold energies for producing these nuclear lines are ≥ 2.5 MeV, the spectrum below that energy is unknown. In estimating the energy in accelerated ions, we normalize to the nuclear fluence in the 4–7 MeV range, $(163 \pm 14) \gamma \text{ cm}^{-2}$ [Lin et al., 2003]. Assuming that the ion spectrum continues unbroken down to 2.5 MeV Nucleon $^{-1}$ and is flat below that energy, we estimate that the flare-accelerated protons contained $(1.0\text{--}4.0) \times 10^{30}$ ergs of energy. This is likely to be a lower limit to the energy in protons; e.g., if the proton spectrum were to continue down

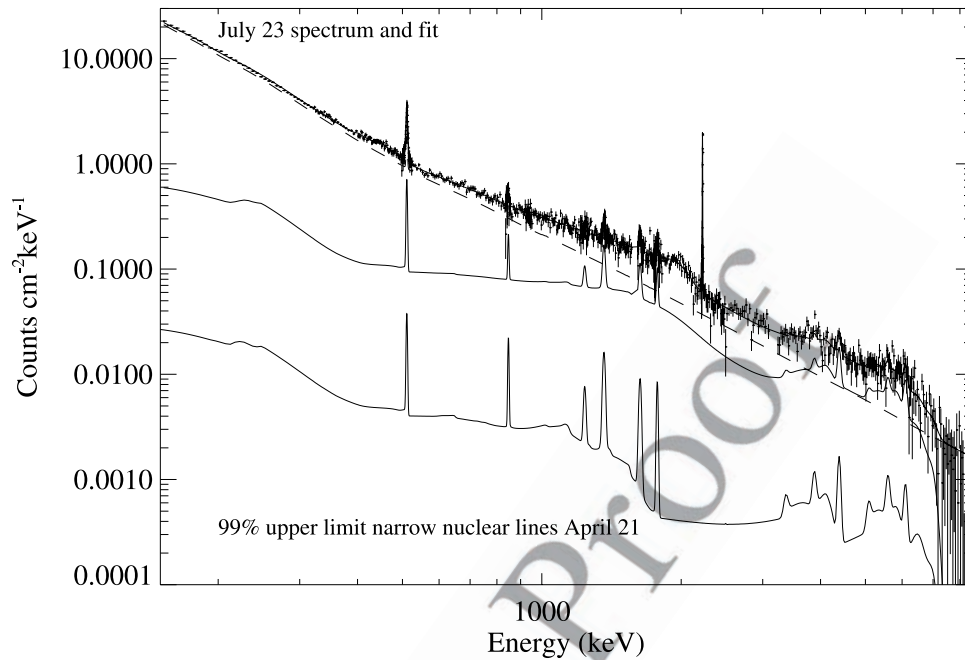


Figure 5. Spectrum of the 23 July flare with the best fit overplotted. The dashed curve is the bremsstrahlung component; the solid curve is the total nuclear component. The 99% confidence limit on the moderately broadened nuclear line component for the 21 April flare is shown for comparison.

to 1 MeV without a break, the energy contained in protons would increase to $(4\text{--}40) \times 10^{30}$ ergs; if the power law extended down to 0.1 MeV, this energy would increase to $(1.2\text{--}120) \times 10^{32}$ ergs. Under the further assumption of “impulsive flare” abundances [Ramaty *et al.*, 1996] and with accelerated $\alpha/p = 0.5$, $\alpha/O = 50$, and ${}^3\text{He}/{}^4\text{He} = 1$, we can estimate the total energy content in protons and heavier ions. For a power law spectrum unbroken down to 2.5 MeV Nucleon $^{-1}$ and flat below that energy, that energy is $U_i \simeq (6\text{--}24) \times 10^{30}$ ergs. For a power law spectrum unbroken down to 1 MeV Nucleon $^{-1}$ that energy is $U_i \simeq (2.4\text{--}24) \times 10^{31}$ ergs; for a low-energy cutoff of 0.1 MeV Nucleon $^{-1}$ it is $U_i \simeq (7\text{--}700) \times 10^{32}$ ergs.

[39] No significant γ -ray line emission was produced in the 21 April 2002 flare; bremsstrahlung emission during that event was only observed up to ~ 350 keV. We have obtained an upper limit on the energy in accelerated ions during the flare by fitting the γ -ray count spectrum with a nuclear-line template and a power law bremsstrahlung component. In order to reduce systematic effects due to background, we have only used our fit to the moderately broadened nuclear deexcitation lines in our determination of the upper limit to the energy. We plot our fit to this component in Figure 5 relative to the total nuclear component fit to the 23 July flare. From this fit we obtain a 99% confidence upper limit of $3.7 \gamma \text{ cm}^{-2}$ on the fluence in the moderately broadened 4.439 MeV ${}^{12}\text{C}$ line. Under the assumption that the power law index of accelerated ions was 4.5 down to 2.5 MeV and is flat at lower energies, and normalizing to the ${}^{12}\text{C}$ line fluence, we obtain 99% confidence upper limits of $U_i \simeq 4.0 \times 10^{30}$ ergs in accelerated ions. For a spectrum unbroken down to 1 MeV Nucleon $^{-1}$ that limit becomes $U_i \simeq 4 \times 10^{31}$ ergs; for a low-energy

limit of 0.1 MeV Nucleon $^{-1}$ the limit is $U_i \simeq 1.2 \times 10^{34}$ ergs.

5. Energetics of Interplanetary Particles

[40] In addition to the kinetic energy of the CME (section 2) and the energy contained in the thermal plasma and in the accelerated particles that interact in the solar atmosphere (sections 3 and 4), energetic particles that escape from the Sun or are accelerated in interplanetary space represent another significant contribution to the global energy budget. These solar energetic particles (SEPs) can be accelerated at the flare site and/or at shocks driven by the CME and can fill a significant part of the heliosphere. Shock acceleration processes, responsible for a vast majority of SEPs, are expected to depend on the strength of the accelerating shock, as well as on the orientation of the shock normal relative to the magnetic field direction. The resulting observed particle spectra in the heliosphere depend strongly on the magnetic connectivity of the observer to the acceleration site [Cane *et al.*, 1988]. The average heliospheric magnetic field geometry is a Parker spiral, which tends to provide better connections to westerly solar longitudes. However, there are observed large-scale deviations of the magnetic field throughout the heliosphere which makes it very difficult to predict magnetic connectivity. In addition, the particle transport may not be completely field-aligned [Giacomini and Jokipii, 1999], which leads to additional complications.

[41] The 23 July event occurred near the east limb of the Sun (S13E72) and, as is typical for east limb events, was apparently not magnetically well connected to Earth. Near-Earth spacecraft such as ACE and GOES did not observe significant energetic particle fluxes that could be traced to

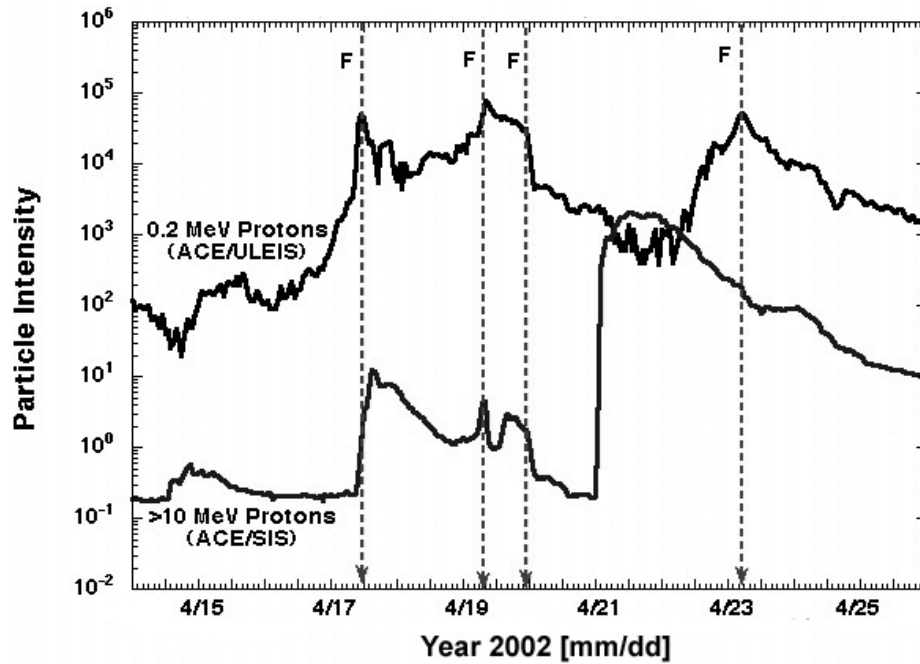


Figure 6. Ion flux as a function of time as measured by ACE/SIS [Stone *et al.*, 1998] and ACE/ULEIS [Mason *et al.*, 1998] for mid-April 2002. The arrival times of forward shocks are indicated.

this event (although interplanetary SEPs from the 23 July event could have been masked by those from an east limb event on 22 July that did produce SEPs at Earth). On the other hand, the 21 April event, at west longitude 84° and south latitude 14° was relatively well connected to Earth, and indeed, a strong interplanetary shock (Mach number $M_A = 3.7$) was observed some 2 days later, at ~ 0415 UT on 23 April. The intensity of 0.2 MeV and >10 MeV protons from 14 April through 26 April is shown in Figure 6. The arrival times of fast forward shocks are also indicated. The intensities of the 0.2 MeV (and to a lesser extent the >10 MeV) peak around the time of shock arrival indicating that acceleration is taking place locally at the shocks.

[42] There is a sharp increase in the >10 MeV proton flux on 21 April within ~ 25 min of the release of a very fast (~ 2500 km s^{-1}) CME and an X1.5 flare, indicating a very good magnetic connection. Note that the maximum in the 0.2 MeV proton intensity did not occur until 23 April, more than a day later than these ions would be expected from velocity-dispersion considerations (low-energy ions travel more slowly along field lines than higher-energy ions). It is possible that low-energy ions accelerated close to the Sun were trapped behind the CME-driven shock and did not reach maximum intensity until the shock arrived. This event appears to be a classic example of a gradual event that is dominated by shock-accelerated rather than flare-accelerated particles, as evidenced by its composition (slightly Fe-poor), its time profile, and also the time profile of the associated X-ray flare (see Figure 1).

[43] Figure 7 shows the fluence spectrum (intensity integrated over the period from 21 April to 25 April) for protons, helium, oxygen, neon, and iron. H and He are the most abundant elements in the SEP population, with heavier

ions up though Fe and Ni accelerated to similar energy per nucleon with roughly coronal abundances. The spectra of all ion species appear to consist of two populations: a power law portion at low energies (<5 MeV nucleon $^{-1}$) that peaks at the time of the shock arrival and exponential spectra at higher energies (e-folding energy ~ 12 MeV for protons) whose intensity peaks early on 21 April.

[44] Daily electron fluences for the 3 days (21 to 23 April) with the highest intensity are shown in Figure 8, including data from ACE/EPAM (red line) and SAMPEX/PET (blue line). The electron time history (not shown) indicates that most of the electrons were accelerated close to the Sun, with only a small contribution from local acceleration when the shock arrives on 23 April.

[45] It is relatively straightforward to integrate the differential energy spectra in Figures 7 and 8 to obtain the total particle energy incident per cm^2 at 1 AU. The limits of this integration were taken to be 10 keV (or keV nucleon $^{-1}$) to infinity. The ion spectra (Figure 7) were extrapolated using the observed power law behavior at low energy and observed exponential behavior at high energy. The electron spectra were extrapolated as power laws at both low and high energy (Figure 8). Overall, about 50% of the contributions are from ~ 0.1 to 100 MeV nucleon $^{-1}$ where there are good observations, and the rest are extrapolated. To relate these fluences to the total energy content of energetic particles, it is necessary to take into account that a given particle may have crossed 1 AU several times due to the diffusive nature of the particle propagation so that particles at 1 AU may have multiple opportunities to be counted. Simulations by J. Giacalone (personal communication, 2002) [see also Li *et al.*, 2003] using scattering mean free paths of ~ 0.01 to 1 AU indicate that the probability of crossing 1 AU more than once is energy dependent, with

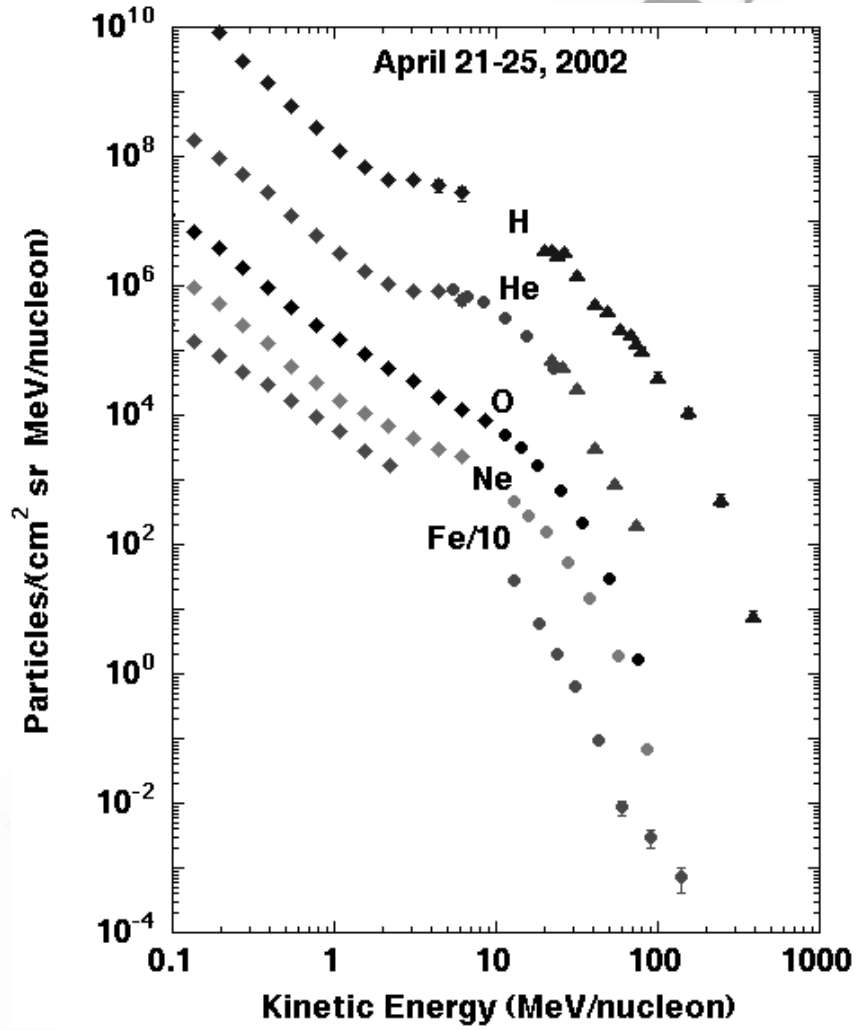


Figure 7. Energy spectra of five species integrated over the period 21–25 April 2002. Included are $2 \leq Z \leq 26$ measurements from ACE/ULEIS [Mason *et al.*, 1998] and ACE/SIS [Stone *et al.*, 1998] and H and He data ($>20 \text{ MeV nucleon}^{-1}$) from SAMPEX/PET [Cook *et al.*, 1993].

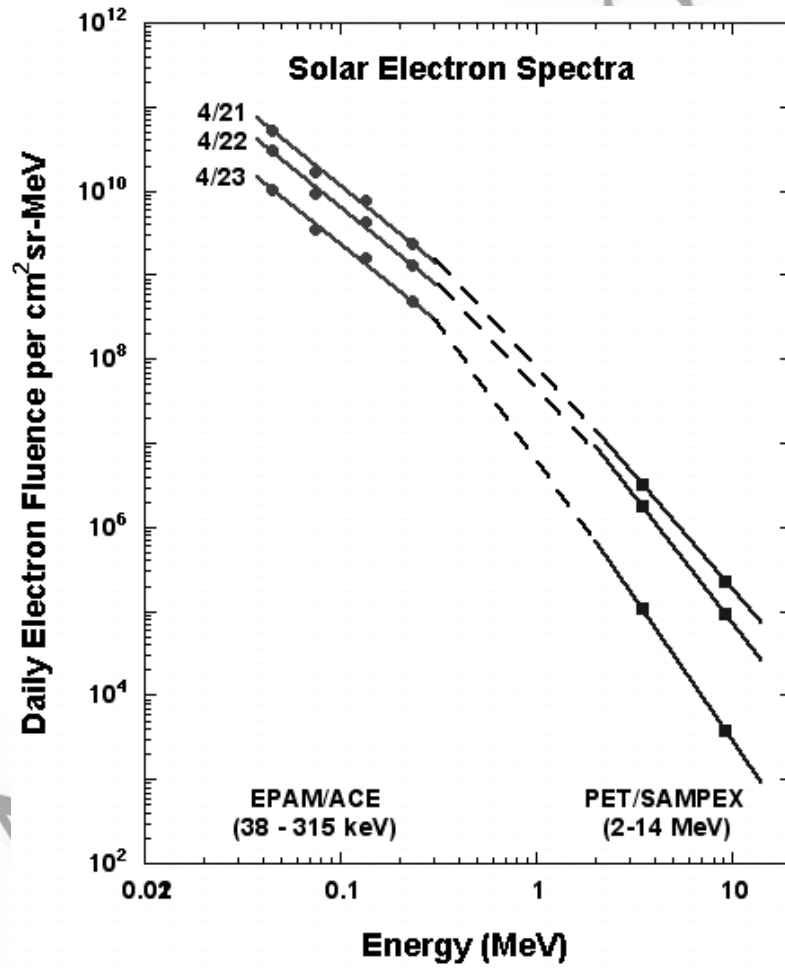


Figure 8. Daily electron fluence measured by ACE/EPAM [Gold *et al.*, 1998] and SAMPEX/PET [Cook *et al.*, 1993] during 21–23 April 2002.

Table 2. Interplanetary Solar Particle Energy Content by Species

Species	Energy Content, ergs	Fraction of Total
Protons	2.3×10^{31}	0.817
Helium	1.8×10^{30}	0.064
$3 \leq Z \leq 28$	4.4×10^{29}	0.016
Electrons	2.9×10^{30}	0.103
Sum	2.8×10^{31}	1.000

typical values ranging from ~ 1 crossing at 0.01 MeV, to ~ 3 crossings at 0.1 MeV, to ~ 7 crossings for 10 MeV protons. We have corrected for this probability using a rigidity-dependent, mean-free path adapted from *Droege* [2001], taking into account the instrument fields of view (e.g., the ACE/SIS and ACE/ULEIS instruments view only in the Sun-facing hemisphere). The result is that because of the multiple crossings, the shock needs to accelerate only about half as many particles as we count in our observations, and the particle energy content needed to produce the observed energy per cm^2 is reduced by a factor of ~ 2 .

[46] To obtain the total energy contained in interplanetary particles, we must also estimate the surface area through which energetic particles escape. Noting that this shock, apparently centered near $W84^\circ$, was still accelerating particles when it reached Earth, we obtain a lower limit to this surface area by assuming that the particles are accelerated uniformly on field lines over a solid angle of $\sim \pi$ ster (in other words, assuming that the measured erg/cm^2 at Earth applies over an area of $\pi \text{ AU}^2$).

[47] However, historically, the largest events at 1 AU are those near the central meridian where the nose of the shock passes by Earth (e.g., the 14 July 2000 and 28 October 2003 events from this solar cycle). Indeed, the five largest >10 MeV proton events from 1976 to 2003 (see the NOAA/GOES catalog at <http://umbra.nascom.nasa.gov/SEP/seps.html>) all originated between $E30^\circ$ and $W30^\circ$ and only one of the top ten is west of $W40^\circ$. By comparison, the 21 April 2002 event (at $W84^\circ$) had a near-Earth fluence that was only $\sim 10\%$ of that of the 14 July 2000 and 28 October 2003 central meridian events, although the CME velocities were comparable. This suggests that a correction should be applied to the observed 21 April 2002 fluence to account for its location relative to Earth. We assume a simple model (inspired by the 1997–2003 longitude distribution of >12 MeV O and Si fluences from ACE and the 1976–2003 longitude distribution of >10 MeV proton events from GOES) in which the fluence is a maximum when the CME is launched from the same latitude and longitude as Earth, falling off exponentially with latitude with an e-folding separation of 35° and with longitude with an e-folding separation of 45° for western events and 25° for eastern events. We can then relate the measured fluence at Earth to the total fluence integrated over longitude and latitude. These e-folding separations are similar in magnitude to those obtained by *Van Hollebeke et al.* [1975], *Kahler* [1982], and *Mason et al.* [1984], although with their smaller data sets they did not deduce that the largest events originate near the central meridian. With these corrections, the global intensity of >10 MeV protons (as measured by GOES) in the 21 April 2002 event is $\sim 45\%$ of that in the 14 July 2000 event and $\sim 29\%$ of that in the 28 October 2003 event. This correction raises the estimated energy content of interplanetary particles in the

21 April 2002 event by a factor of ~ 5 compared with the lower limit estimated above.

[48] The total energy content of the interplanetary particles is summarized by species in Table 2, including the corrections for longitude and latitude discussed above. With these corrections, the 21 April event becomes the seventh largest >10 MeV proton event of this solar cycle, and its fluence is now more on a par with that of other large events. Note that the total energy in energetic particles (2.8×10^{31} ergs) is a significant fraction ($\sim 15\%$) of the CME kinetic energy ($\sim 1.8 \times 10^{32}$ ergs), implying that shock acceleration must be relatively efficient.

[49] By far the largest uncertainty in the energy budget for energetic particles at 1 AU (U_p in Table 2) is in the procedure for relating the fluences at Earth to the total interplanetary particle population because of uncertainties in the longitude and latitude intensity distributions. We estimate this uncertainty to be a factor of ~ 3 . There is also an uncertainty of $\Delta \log_{10} U_p \simeq 0.2$ in the correction for how many times particles cross 1 AU. The relative contribution of the various species are much better known, to perhaps 30% for the ions and $\sim 50\%$ for electrons. All of these uncertainties are independent, but the overall uncertainty in the energy content of the accelerated interplanetary particles could be as large as a factor of four.

6. Magnetic Energy

[50] The magnetic energy associated with coronal currents is generally considered to be the source of the thermal, kinetic, and radiative energy released in a flare or CME event. This magnetic energy can be expressed as

$$\frac{1}{8\pi} \int_{r>R_0} (B^2 - B_p^2) dV, \quad (5)$$

where B is the strength of the total magnetic field, B_p is the strength of the potential magnetic field produced by sources below the corona, r is the radial coordinate, and R_0 is the lower boundary of the corona.

[51] Using the MHD virial theorem [*Chandrasekhar and Fermi*, 1953; *Chandrasekhar*, 1961; *Molodenskii*, 1969; *Aly*, 1984, 1989; *Low*, 1984, 1999; *Litvinenko and Somov*, 2001], one can express the total magnetic energy in terms of the field components at the lower boundary of the corona as

$$\begin{aligned} U_B &= \frac{1}{8\pi} \int_{r>R_0} B^2 dV \\ &= \frac{R_0}{8\pi} \int_{r=R_0} (B_r^2 - B_\theta^2 - B_\phi^2) dS - \int_{r=R_0} p dS \\ &\quad + \int_{r>R_0} \left(\frac{\rho G M_0}{r} - 3p \right) dV, \end{aligned} \quad (6)$$

where B_r , B_θ , and B_ϕ are the spherical components of the total field B , p is the coronal gas pressure, ρ is the coronal density, G is the universal constant of gravitation, M_0 is the solar mass, and dS is the differential surface element. If the gravitational and thermal energy terms are ignored, then the field is force-free, and the magnetic energy available to drive the eruption is given entirely in terms of an integral over the components of the surface field. During the timescale of an eruption the radial component of the magnetic field is essentially constant because of inertial line

t3.1 **Table 3.** CME/Flare Energy Budgets for the 21 April 2002 and
23 July 2002 Events

t3.2	Mode	Symbol	\log_{10} (Energy, erg)	
			21 April 2002	23 July 2002
t3.4	Magnetic Flare	U_B	32.3 ± 0.3	32.3 ± 0.3
t3.5	Thermal plasma, $T > 10$ MK	U_{th}	$31.3^{+0.4}_{-1}$	$31.1^{+0.4}_{-1}$
t3.6	Nonthermal electrons	U_e	$31.3^{+0.5}_{-0.5}$	$31.5^{+0.5}_{-0.5}$
t3.7	Nonthermal ions, >1 MeV nucleon $^{-1}$	U_i	<31.6	31.9 ± 0.5
CME				
t3.9	Kinetic	U_K	32.3 ± 0.3	32.0 ± 0.3
t3.10	Gravitational potential	U_Φ	30.7 ± 0.3	31.1 ± 0.3
t3.11	Energetic particles at 1 AU	U_p	31.5 ± 0.6	none above background

781 tying, which constrains the outward magnetic flux to the same
782 surface area at the photosphere. Therefore if the effects of gas
783 pressure and gravity are negligible, equation (6) implies an
784 upper limit on the total magnetic energy, U_B , because ($B_0^2 +$
785 B_ϕ^2) must be somewhere in the range between its potential
786 value and zero. For a simple dipole field the upper limit on the
787 total energy set by the virial theorem is twice the potential
788 energy. Other distributions of the surface field tend to give
789 somewhat higher values [see *Wolfson*, 2003].

790 [52] Owing to the constraints imposed by helicity con-
791 servation, not all of the “free” magnetic energy may be
792 available on short timescales to power flares and CMEs;
793 however, it does provide an upper limit on the magnitude of
794 the energy available. If the helicity of the field were known,
795 one could subtract the energy of the equivalent linear force-
796 free field with the same helicity rather than the energy of the
797 potential field as was done above.

798 [53] Unfortunately, the chromospheric vector magnetic
799 field observations required to apply the magnetic virial
800 theorem are not available for the 21 April and 23 July
801 events. While in principle it is possible to compute the
802 potential field energy from the MDI line-of-sight magneto-
803 grams, in practice the active regions which produced the 21
804 April and 23 July events were too close to the limb for such
805 a calculation. However, other large active regions similar to
806 those involved in the 21 April and 23 July events contain
807 some 10^{33} ergs in nonpotential (free) magnetic energy
808 [Metcalf *et al.*, 1995, 2002]. For example, in AR 7216
809 analyzed by Metcalf *et al.* [1995], the free magnetic energy
810 is $U_B = (1.2 \pm 0.2) \times 10^{33}$ ergs, which is about one third of
811 the total magnetic energy in AR7216 ($U_B = (3.2 \pm 0.2) \times$
812 10^{33} ergs). A free energy of 10^{33} ergs is some 5 times the
813 total energy budget of the 21 April and 23 July events,
814 demonstrating that the conversion of roughly 20% of the
815 available free energy is required to power these events.

816 7. Putting it All Together: Energy Partition in the 817 Two Events

818 [54] Table 3 shows the combined results of the previous
819 sections, in the form $\log_{10}U \pm \Delta\log_{10}U$, for each energy
820 component. Figure 9 shows the summary results for the
821 23 July event in pictorial form.

822 [55] We should note at the outset that the uncertainties in
823 all the measured quantities are large. For example, as
824 pointed out in section 4, the energy in accelerated ions is

uncertain by several orders of magnitude because of the
unknown lower limit to the accelerated ion spectrum (we
show results for a lower limit of 1 MeV in Table 3). Also,
not all these energy contents are independent: for example,
the energy in nonthermal electrons is converted through
Coulomb collisions into energy in the thermal plasma.
Hence one should not simply sum these individual compo-
nents up to get a “total” energy for the event.

[56] Notwithstanding these remarks, however, a few
(cautious) remarks can still be made. First, it is clear that
in both events the coronal mass ejection has the dominant
component of the released energy, and furthermore, it
contains a substantial fraction (30%) of the available mag-
netic energy. Second, the energy in accelerated electrons is
comparable to that in accelerated ions. Third, at least for the
low-energy spectral cutoffs used herein, both electron and
ion energies are a half to a whole order of magnitude
smaller than the energy contained in the CME. Fourth, the
peak energy in the thermal soft X-ray plasma is about an
order of magnitude less than the energy in the accelerated
(electrons + ions above 1 MeV); the rest of the energy
deposited by these particles is presumably converted into
radiation in other wavebands (e.g., EUV, optical) (cf.
Canfield et al. [1980] for estimates) and into kinetic energy,
perhaps of the CME itself. Fifth and finally, the energy in
interplanetary particles accelerated by the CME shock in the
21 April event is some 15% of the energy in the CME itself,
an indication of the acceleration efficiency of the interplan-

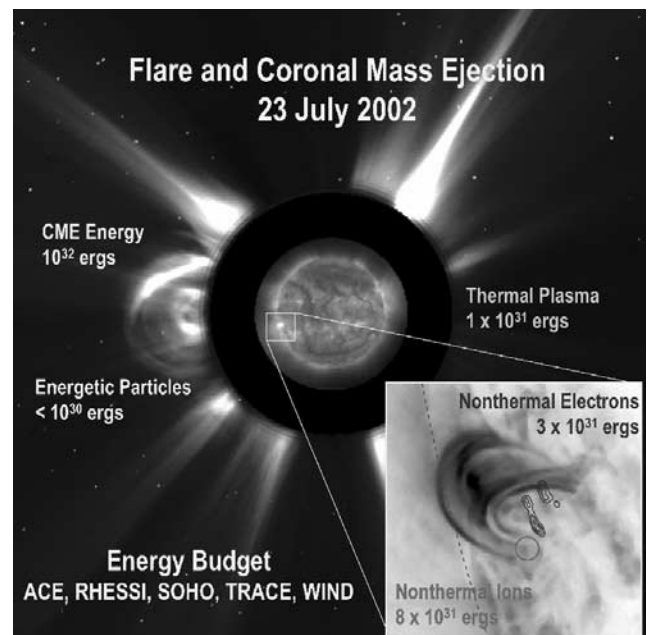


Figure 9. Summary of the morphology and energetics of the 23 July event. The main frame shows the coronal mass ejection structure in LASCO, together with an EIT 195 Å image of the Sun. The expanded region at the lower right shows the hard X-ray (50–100 keV) contours, the centroid of the 2.223 MeV line emission (circle), and the postflare loops as observed by TRACE. The best estimates for the energies of the various components are indicated directly on the figure. See color version of this figure at back of this issue.

etary shock. We encourage the development of theoretical estimates against which to assess this result.

[57] **Acknowledgments.** The Taos Workshop was supported in part by NASA and the Los Alamos National Laboratory. AGE was supported by NASA grant NAG5-207445 through the University of California, Berkeley. RJM and GHS were supported by NASA grants DPR W19746 and S13377G. TRM was supported in part by NASA grant NAG5-12466. The energetic particle work was supported by NASA grants NAS5-12929 at Caltech and the University of Maryland and by NASA grant NAS5-12929 at the University of New Hampshire. RAM appreciates the assistance of Mark Looper, Christina Cohen, and the availability of data from the ACE/EPAM instrument through the ACE Science Center.

[58] Shadia Rifai Habbal thanks Richard C. Canfield and another referee for their assistance in evaluating this paper.

References

Aly, J. J. (1984), On some properties of force-free magnetic fields in infinite regions of space, *Astrophys. J.*, **283**, 349.

Aly, J. J. (1989), On the reconstruction of the nonlinear force-free coronal magnetic field from boundary data, *Sol. Phys.*, **120**, 19.

Aschwanden, M. J., and C. E. Parnell (2002), Nanoflare statistics from first principles: Fractal geometry and temperature synthesis, *Astrophys. J.*, **572**, 1048.

Brown, J. C. (1973), Thick target X-ray bremsstrahlung from partially ionised targets in solar flares, *Sol. Phys.*, **28**, 151.

Brown, J. C., and A. G. Emslie (1988), Analytic limits on the forms of spectra possible from optically thin collisional bremsstrahlung source models, *Astrophys. J.*, **331**, 554.

Brown, J. C., A. G. Emslie, and E. P. Kontar (2003), The determination and use of mean electron flux spectra in solar flares, *Astrophys. J. Lett.*, **595**, L115.

Brueckner, G. E., et al. (1995), The Large Angle Spectroscopic Coronagraph (LASCO), *Sol. Phys.*, **162**, 357.

Cane, H. V., D. V. Reames, and T. T. von Rosenvinge (1988), The role of interplanetary shocks in the longitude distribution of solar energetic particles, *J. Geophys. Res.*, **93**, 9555.

Canfield, R. C., C.-C. Cheng, K. P. Dere, G. A. Dulk, D. J. McLean, E. J. Schmahl, R. D. Robinson Jr., and S. A. Schoolman (1980), Radiative energy output of the 5 September 1973 flare, in *Solar Flares: A Monograph From Skylab Solar Workshop II*, edited by P. A. Sturrock, p. 451, Colo. Assoc. Univ. Press, Boulder, Colo.

Chandrasekhar, S. (1961), *Hydrodynamic and Hydromagnetic Stability*, Dover, New York.

Chandrasekhar, S., and E. Fermi (1953), Problems of gravitational stability in the presence of a magnetic field, *Astrophys. J.*, **119**, 116.

Cook, W. R., A. C. Cummings, J. R. Cummings, T. L. Garrard, B. Kerman, R. A. Mewaldt, R. S. Selesnick, E. C. Stone, and T. T. von Rosenvinge (1993), PET: A Proton/Electron Telescope for studies of magnetospheric, solar, and galactic particles, *IEEE Trans. Geosci. Remote Sens.*, **31**, 565.

de Jager, C., M. E. Bruner, C. J. Crannell, B. R. Dennis, J. R. Lemen, and S. F. Martin (1986), Energetics of the impulsive phase, in *Energetic Phenomena on the Sun: The Solar Maximum Mission Workshop Proceedings*, NASA Conf. Proc. 2439, pp. 5-5–5-20, NASA, Washington, D. C.

Dennis, B. R., et al. (2003), The Neupert effect and new RHESSI measures of the total energy in electrons accelerated in solar flares, *Adv. Space Res.*, **32**, 2459.

Domingo, V., B. Fleck, and A. I. Poland (1995), The SoHO Mission: An overview, *Sol. Phys.*, **162**, 1.

Droege, W. (2001), Can we predict transport coefficients of heliospheric particles from solar wind observations?, *27th Int. Cosmic Ray Conf.*, **8**, 3285.

Emslie, A. G. (1978), The collisional interaction of a beam of charged particles with a hydrogen target of arbitrary ionization level, *Astrophys. J.*, **224**, 241.

Gallagher, P. T., B. R. Dennis, S. Krucker, R. A. Schwartz, and A. K. Tolbert (2002), RHESSI and TRACE observations of the 21 April 2002 X1.5 flare, *Sol. Phys.*, **210**, 341.

Gallagher, P. T., G. R. Lawrence, and B. R. Dennis (2003), Rapid acceleration of a coronal mass ejection in the low corona and implications for propagation, *Astrophys. J. Lett.*, **588**, L53.

Giagalone, J., and J. R. Jokipii (1999), The transport of cosmic rays across a turbulent magnetic field, *Astrophys. J.*, **520**, 204.

Gold, R. E., S. M. Krimigis, S. E. Hawkins III, D. K. Haggerty, D. A. Lohr, E. Fiore, T. P. Armstrong, G. Holland, and L. J. Lanzerotti (1998), Electron, proton and alpha monitor on the Advanced Composition Explorer spacecraft, *Space Sci. Rev.*, **86**, 541.

Haug, E. (1997), On the use of nonrelativistic bremsstrahlung cross sections in astrophysics, *Astron. Astrophys.*, **326**, 417.

Holman, G. D. (2003), The effects of low- and high-energy cutoffs on solar flare microwave and hard X-ray spectra, *Astrophys. J.*, **586**, 606.

Holman, G. D., L. Sui, R. A. Schwartz, and A. G. Emslie (2003), Electron bremsstrahlung hard X-ray spectra, electron distributions, and energetics in the 2002 July 23 solar flare, *Astrophys. J. Lett.*, **595**, L97.

Hurford, G. J., et al. (2002), The RHESSI imaging concept, *Sol. Phys.*, **210**, 61.

Kahler, S. W. (1982), The role of the big flare syndrome in correlations of solar energetic proton fluxes and associated microwave burst parameters, *J. Geophys. Res.*, **87**, 3439.

Kontar, E. P., J. C. Brown, and G. K. McArthur (2002), Nonuniform target ionization and fitting thick-target electron injection spectra to RHESSI data, *Sol. Phys.*, **210**, 419.

Li, G., G. P. Zank, and W. K. M. Rice (2003), Energetic particle acceleration and transport at coronal mass ejection-driven shocks, *J. Geophys. Res.*, **108**(A2), 1082, doi:10.1029/2002JA009666.

Lin, R. P., et al. (2003), RHESSI observations of particle acceleration and energy release in an intense solar gamma-ray line flare, *Astrophys. J. Lett.*, **595**, L69.

Litvinenko, Y. E., and B. V. Somov (2001), Aspects of the global MHD equilibria and filament eruptions in the solar corona, *Space Sci. Rev.*, **95**, 67.

Low, B. C. (1984), Modeling solar magnetic structures, in *Measurements of Solar Vector Magnetic Fields*, NASA CP 2374, edited by M. J. Hagyard, p. 49, NASA, Washington, D. C.

Low, B. C. (1999), Coronal mass ejections, flares and prominences, in *Solar Wind Nine*, edited by S. R. Habbal et al., *AIP Conf. Proc.*, **471**, 109.

Mason, G. M., G. Gloeckler, and D. Hovestadt (1984), Temporal variations of nucleonic abundances in solar flare energetic particle events. II Evidence for large-scale shock acceleration, *Astrophys. J.*, **280**, 902.

Mason, G. M., et al. (1998), The Ultra Low Energy Isotope Spectrometer (ULEIS) for the ACE spacecraft, *Space Sci. Rev.*, **86**, 409.

Metcalf, T. R., L. Jiao, H. Uitenbroek, A. N. McClymont, and R. C. Canfield (1995), Is the solar chromospheric magnetic field force-free?, *Astrophys. J.*, **439**, 474.

Metcalf, T. R., D. L. Mickey, B. J. LaBonte, and L. A. Ryder (2002), The magnetic free energy and a CME in active region 8299, in *Multi-Wavelength Observations of Coronal Structure and Dynamics*, COSPAR Colloq. Ser., vol. 13, edited by P. C. H. Martens and D. P. Cauffman, p. 249, Elsevier Sci., New York.

Molodenskii, M. M. (1969), Integral properties of force-free fields, *Sov. Astron., Engl. Transl.*, **12**, 585.

Moore, R. L., D. L. McKenzie, Z. Svestka, K. G. Widing, K. P. Dere, S. K. Antiochos, H. W. Dodson-Prince, E. Hiei, K. R. Krall, and A. S. Krieger (1980), The thermal X-ray flare plasma, in *Solar Flares: A Monograph From Skylab Solar Workshop II*, edited by P. A. Sturrock, pp. 341–409, Colo. Assoc. Univ. Press, Boulder, Colo.

Neupert, W. M. (1968), Comparison of solar X-ray line emission with microwave emission during flares, *Astrophys. J.*, **153**, 59.

Phillips, K. J. H. (2004), The solar flare 3.8–10 keV X-ray spectrum, *Astrophys. J.*, **605**, 921.

Poland, A. I., R. A. Howard, M. J. Koomen, D. J. Michels, and N. R. Sheeley (1981), Coronal transients near sunspot maximum, *Sol. Phys.*, **69**, 169.

Ramaty, R., and N. Mandzhavidze (2000), Gamma-rays from solar flares, in *Highly Energetic Physical Processes and Mechanisms for Emission from Astrophysical Plasmas*, ASP Conf. Ser., **195**, edited by P. C. H. Martens, S. Tsuruta, and M. A. Weber, p. 123, Astron. Soc. of the Pac., Provo, Utah.

Ramaty, R., B. Kozlovsky, and R. Lingenfelter (1979), Nuclear gamma-rays from energetic particle interactions, *Astrophys. J. Suppl.*, **40**, 487.

Ramaty, R., N. Mandzhavidze, and B. Kozlovsky (1996), Solar atmospheric abundances from gamma-ray spectroscopy, in *High Energy Solar Physics*, AIP Conf. Proc., vol. 374, edited by R. Ramaty, N. Mandzhavidze, and X.-M. Hua, p. 172, Am. Inst. of Phys., New York.

Reeves, K. K., and H. P. Warren (2002), Modeling the cooling of postflare loops, *Astrophys. J.*, **578**, 590.

Saint-Hilaire, P., and A. O. Benz (2002), Energy budget and imaging spectroscopy of a compact flare, *Sol. Phys.*, **210**, 287.

Schmahl, E. J., and G. J. Hurford (2002), RHESSI observations of the size scales of solar hard X-ray sources, *Sol. Phys.*, **210**, 273.

Smith, D. F., and C. G. Lilliequist (1979), Confinement of hot, hard X-ray producing electrons in solar flares, *Astrophys. J.*, **232**, 582.

Stone, E. C., et al. (1998), The Solar Isotope Spectrometer for the Advanced Composition Explorer, *Space Sci. Rev.*, **86**, 357.

Strong, K. T., A. O. Benz, B. R. Dennis, J. W. Leibacher, R. Mewe, A. I. Poland, J. Schrijver, G. Simnett, J. B. Smith Jr., and J. Sylwester (1984), A multiwavelength study of a double impulsive flare, *Sol. Phys.*, **91**, 325.

- 1008 Strong, K. T., et al. (1986), Energetics of the gradual phase, in *Energetic*
 1009 *Phenomena on the Sun: The Solar Maximum Mission Workshop Pro-*
 1010 *ceedings, NASA Conf. Proc. 2439*, pp. 5-20–5-39, NASA, Washington,
 1011 D. C.
 1012 van Hollebeke, M. A. I., L. S. Ma Sung, and F. B. McDonald (1975), The
 1013 variation of solar proton energy spectra and size distribution with helio-
 1014 longitude, *Solar Phys.*, *41*, 189.
 1015 Vourlidas, A., P. Subramanian, K. P. Dere, and R. A. Howard (2000),
 1016 Large-angle spectrometric coronagraph measurements of the energetics
 1017 of coronal mass ejections, *Astrophys. J.*, *534*, 456.
 1018 Vourlidas, A., et al. (2002), Mass and energy properties of LASCO
 1019 CMEs, in *Proceedings of the 10th European Solar Physics Meeting—*
 1020 *Solar Variability: From Core to Outer Frontiers, ESA SP-506*, edited by
 1021 A. Wilson, p. 91, Eur. Space Agency, Paris.
 1022 Wolfson, R. (2003), Role of magnetic flux distribution in coronal energy
 1023 storage, *Astrophys. J.*, *593*, 1208.
- 1024 B. R. Dennis, P. T. Gallagher, G. D. Holman, and R. A. Schwartz, NASA
 1026 Goddard Space Flight Center, Code 682, Greenbelt, MD 20771, USA.
 1027 (brian.r.dennis@nasa.gov; peter.t.gallagher.1@gsfc.nasa.gov; gordon.d.
 1028 holman@nasa.gov; richard.a.schwartz.1@gsfc.nasa.gov)
- A. G. Emslie, Department of Physics, University of Alabama in 1029
 Huntsville, Huntsville, AL 35899, USA. (emslieg@uah.edu) 1030
 T. G. Forbes and H. Kucharek, Institute for the Study of Earth, Oceans, 1031
 and Space, University of New Hampshire, Durham, NH 03824, USA. 1032
 (terry.forbes@unh.edu; kucharek@atlas.sr.unh.edu) 1033
 N. Gopalswamy, NASA Goddard Space Flight Center, Code 695, 1034
 Greenbelt, MD 20771, USA. (gopals@fugee.gsfc.nasa.gov) 1035
 T. R. Metcalf, Lockheed Martin Solar and Astrophysics Laboratory, 1036
 Department L9-41, B252, 3251 Hanover Street, Palo Alto, CA 94304, 1037
 USA. (metcalf@lmsal.com) 1038
 G. M. Mason, Physics Department, University of Maryland, College 1039
 Park, MD 20742, USA. (glenn.mason@umail.umd.edu) 1040
 R. A. Mewaldt, 220-47 Downs Laboratory, California Institute of 1041
 Technology, Pasadena, CA 91125, USA. (rmewaldt@srl.caltech.edu) 1042
 R. J. Murphy and G. H. Share, Naval Research Laboratory, Code 7650, 1043
 4555 Overlook Avenue SW, Washington, DC 20375, USA. (ronald. 1044
 murphy@nrl.navy.mil; gerald.share@nrl.navy.mil) 1045
 A. Vourlidas, Naval Research Laboratory, Code 7663, 4555 Overlook 1046
 Avenue SW, Washington, DC 20375, USA. (avourlid@pythia.nrl.navy.mil) 1047
 T. H. Zurbuchen, Department of Atmospheric, Oceanic and Space 1048
 Sciences, University of Michigan, 2455 Hayward Street, Ann Arbor, MI 1049
 48109, USA. (thomasz@umich.edu) 1050

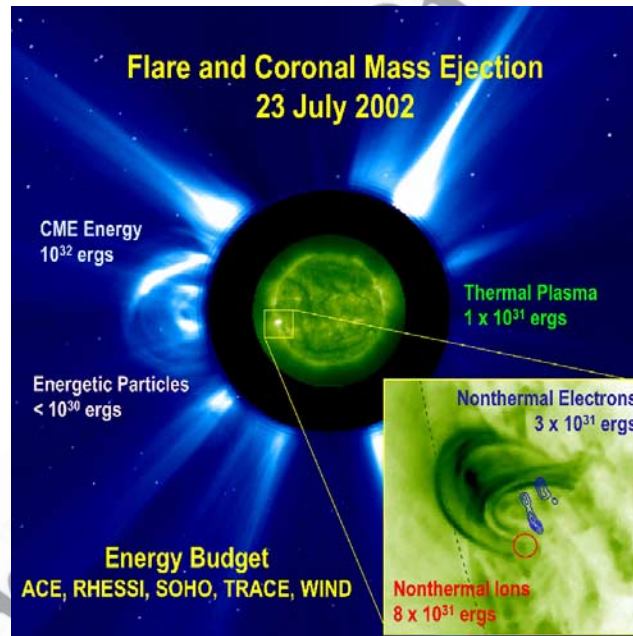


Figure 9. Summary of the morphology and energetics of the 23 July event. The main frame shows the coronal mass ejection structure in LASCO, together with an EIT 195 Å image of the Sun. The expanded region at the lower right shows the hard X-ray (50–100 keV) contours, the centroid of the 2.223 MeV line emission (circle), and the postflare loops as observed by TRACE. The best estimates for the energies of the various components are indicated directly on the figure.